Proceedings of the
Annual Stability Conference
Structural Stability Research Council
St. Louis, Missouri, April 16-20, 2013

Cyclic Lateral-Torsional Buckling Response of Cold-Formed Steel C-Section Joists

D.A. Padilla-Llano[1], C.D. Moen[2], M. Eatherton[3]

Abstract
Design of cold-formed steel (CFS) structures subjected to lateral seismic forces traditionally relies on the cyclic strength of subassemblages such as strapped/sheathed shear walls. Little regard is paid to the behavior of the individual components, their contribution to the lateral resistance of CFS structures, or to the actual seismic behavior of the structure as a whole. Understanding the cyclic behavior at the individual component level is necessary to develop a toolbox of nonlinear elements capable of accurately and efficiently simulating the seismic behavior of the infinite number of possible configurations in cold-formed steel structures. This paper summarizes initial results from an experimental program designed to evaluate the flexural cyclic response of cold-formed steel C-shaped structural flexural members. A cyclic loading protocol is adapted for cold-formed steel members to evaluate the energy dissipation characteristics of members experiencing lateral-torsional buckling deformations.

1. Introduction

This paper experimentally explores the cyclic lateral-torsional buckling response of unbraced cold-formed steel lipped C-section joists. Energy dissipation characteristics and cyclic strength degradation are quantified for two common industry cross-sections. The results presented herein will be used to parameterize the cyclic hysteretic response of cold-formed steel joist in support of a multi-university research effort to develop seismic design guidelines for cold-formed steel framing being led by Johns Hopkins University (Madsen et. al 2011). Hysteretic response curves are needed in the near future as input into high fidelity nonlinear dynamic simulations (e.g., OpenSees). These simulations will be useful for developing and validating seismic design procedures for mid-rise cold-formed steel framed buildings.

To the authors' knowledge, there have only been a few studies on the cyclic performance of cold-formed steel flexural members, and none that specifically isolate lateral-torsional buckling deformation of a single joist as described in this study. Calderoni et al. (2009) tested back-to-back lipped C-sections loaded in three point bending to study local buckling cyclic strength

[1] Graduate Research Assistant, Civil & Environmental Engineering, Virginia Tech, <dapadill@vt.edu>
[2] Assistant Professor, Civil & Environmental Engineering, Virginia Tech, <cmoen@vt.edu>
[3] Assistant Professor, Civil & Environmental Engineering, Virginia Tech,<meather@vt.edu>

degradation. Post-buckling ductility and inelastic energy dissipation were observed, and the authors recommended future studies to take advantage of these potentially beneficial characteristics in seismic events. Hsu and Chi (2003) also performed cyclic tests on back-to-back cold-formed steel lipped C-sections with the goal of demonstrating a design alternative to hot-rolled steel I-beams in mid-rise buildings. Three point cycle bending tests were conducted, and the results demonstrated that inelastic local buckling deformation dissipated more energy than elastic buckling deformation, results consistent with those of Padilla-Llano et al. (2012) who recently studied the cyclic behavior of cold-formed steel stud columns.

The paper begins by explaining the strategy for selecting specimen cross-sections and introducing the test matrix. The test setup is described, including details on how warping-fixed boundary conditions were achieved while accommodating cyclic flexural motion. A modified FEMA 461 loading protocol is employed where the anchor displacements are based on joist global slenderness. The paper concludes with a presentation of the hysteretic curves of specimens experiencing elastic buckling, inelastic buckling, yielding and stiffness loss, and post-buckling strength degradation.

2. Experimental Program Design

The cold-formed steel beam test matrix and measured specimen dimensions are provided in Table 1, with specimen notation provided in Fig. 1. Lipped C-section cross-sections with two different nominal web depths, 203 mm and 305 mm, were considered. Flange width, lip length, base metal thickness, and the beam unbraced length (L_u) were selected to isolate the global buckling flexural strength limit state from local and distortional buckling deformation using the AISI Direct Strength Method (AISI 2007), i.e., $M_{ne}=M_{n\ell}$ and $M_{ne}>>M_{nd}$ for all specimens. Two monotonic tests and two cyclic tests were performed for each cross-section type. The measured out-to-out dimensions, yield stress F_y determined as the average of three tensile coupon tests taken from the flats of the web and two flanges, and elastic buckling parameters for each specimen are provided in Table 2. The critical elastic buckling moment, M_{cre}, was calculated assuming k=0.5, i.e., the joists are warping fixed between brace (load) points.

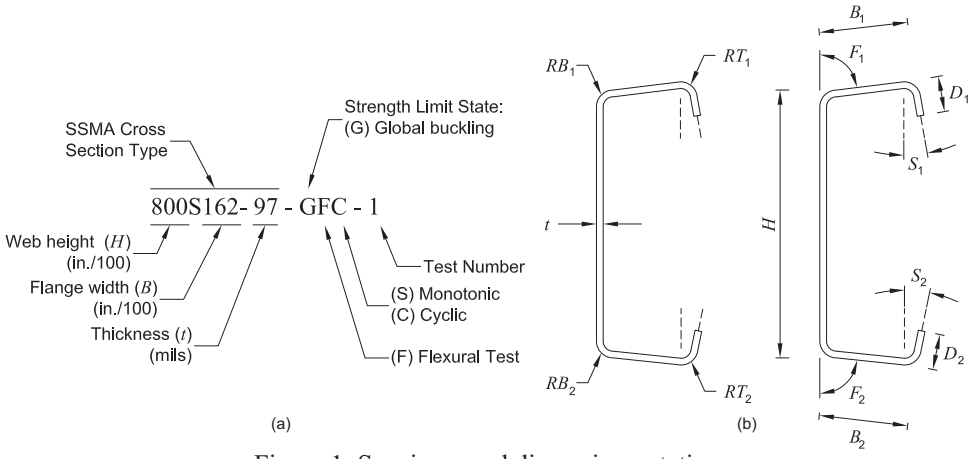

Figure 1: Specimen and dimension notation

Table 1: Measured specimens dimensions

Specimen	L_u	A_g	D_1	D_2	B_1	B_2	H	RT_1	RB_1	RT_2	RB_2	F_1	F_2	S_1	S_2	t
	(mm)	(mm^2)	(mm)	(mm)	(mm)	(mm)	(mm)	(mm)	(mm)	(mm)	(mm)	(°)	(°)	(°)	(°)	(mm)
800S162-97-GFC-1	3048	734	9.7	11.4	42.9	42.5	203.9	4.4	5.6	5.2	5.2	90.6	88.8	-2.3	0.7	2.50
800S162-97-GFC-2	3048	734	12.4	13.0	40.6	40.2	203.9	5.0	5.4	5.2	5.4	90.3	88.8	0.5	2.1	2.50
800S162-97-GFM-1	3048	732	9.9	11.4	42.4	42.3	204.0	4.8	5.4	5.2	5.2	90.6	88.8	-2.7	-1.1	2.50
800S162-97-GFM-2	3048	735	12.2	13.6	40.3	39.9	203.8	4.8	5.4	5.2	5.2	89.0	87.7	0.7	2.1	2.51
1200S162-97-GFC-1	3048	995	9.8	11.3	42.5	43.1	305.7	4.8	5.6	5.2	5.6	91.2	88.0	-2.8	2.6	2.52
1200S162-97-GFC-2	3048	993	10.1	10.9	42.8	43.1	305.7	5.0	5.6	5.2	5.6	90.9	87.5	-2.8	3.0	2.51
1200S162-97-GFM-1	3048	991	10.0	11.1	42.3	43.2	305.9	4.8	5.6	5.2	5.6	91.2	88.2	-3.7	-3.1	2.51
1200S162-97-GFM-2	3048	991	10.8	10.0	42.8	42.0	305.7	5.2	5.6	4.8	5.6	88.7	90.7	2.5	-4.0	2.51

Table 2: Yield stress and elastic buckling properties

Specimen	F_y	M_y	M_n	M_{ne}	M_{nd}	M_{nt}	δ_e
	(MPa)	(kN-mm)					($\times 10^{-3}$mm)
800S162-97-GFC-1	452	17786	10005	10005	15519	10005	6937
800S162-97-GFC-2	454	17752	9854	9854	16124	9854	6867
800S162-97-GFM-1	452	17711	9721	9721	15522	9721	6770
800S162-97-GFM-2	462	18182	9623	9623	16385	9623	6664
1200S162-97-GFC-1	448	32664	15524	15524	22494	15524	3871
1200S162-97-GFC-2	464	33835	15835	15835	23050	15835	3951
1200S162-97-GFM-1	451	32668	15272	15272	22454	15272	3830
1200S162-97-GFM-2	449	32580	15529	15529	22424	15529	3895

3. Test Setup

All tests were conducted in four point bending using a 250kN capacity MTS actuator bolted to a reaction frame made of steel wide flange sections anchored down to a strong floor (Fig. 2). An MTS model 407 controller applied a cyclic displacement history using an external analog input created using a custom control program in Labview (Labview 2012) and National Instruments hardware. The joist span from centerline support to centerline support was L=4877mm. Loading locations and end supports were detailed to resist tension and compression. Loading and support pins pass through slotted holes to prevent axial force from developing in a specimen. Lateral braces were placed in the shear spans to develop longitudinal warping fixity at the loading points. Two LVDTs were used to measure the vertical displacement at the loading points. The average of the two displacements is used for control of the test through the customized control program.

4. Cyclic Loading Protocol

In this study a modification to the FEMA 461 loading protocol (FEMA 2007) is proposed as shown in Fig. 3. The anchor point for the protocol is the beam vertical displacement at a load point, δ_e, calculated as

$$\delta_e = \frac{M_e a}{6EI}(3L - 4a) \tag{1}$$

where a=802mm is the distance from the centerline support to the loading point and L=4877mm is the beam span from centerline support to centerline support. The parameter M_e is the moment expected to initiate flexural-torsional buckling deformation. It is calculated using slenderness limits defined in the AISI Direct Strength Method (AISI 2007). Specifically, the DSM approach dictates global buckling deformation initiates at M_e=0.36M_{cre}. The critical elastic lateral-torsional

buckling moment, M_{cre}, is calculated considering warping fixed boundary conditions at the load points. The anchor displacement, δ_e, is provided for each specimen in Table 2.

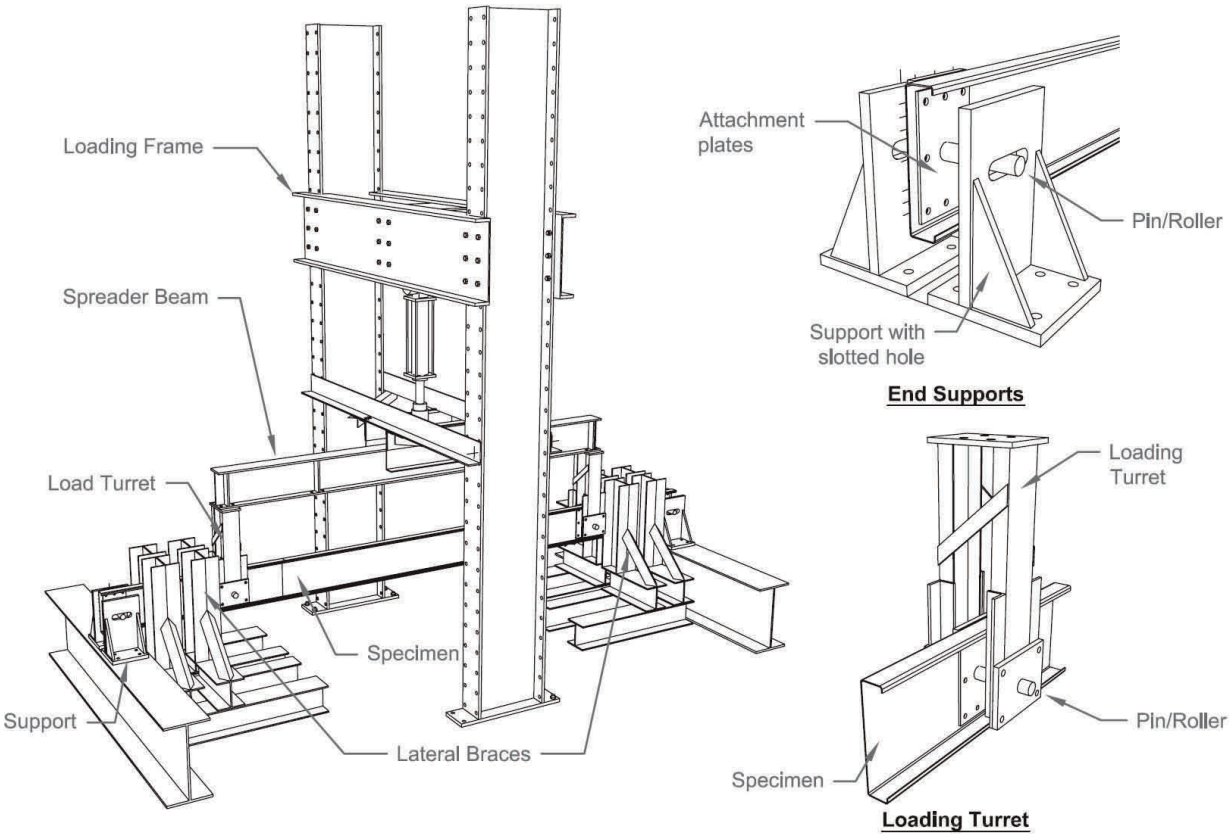

Figure 2: Test setup

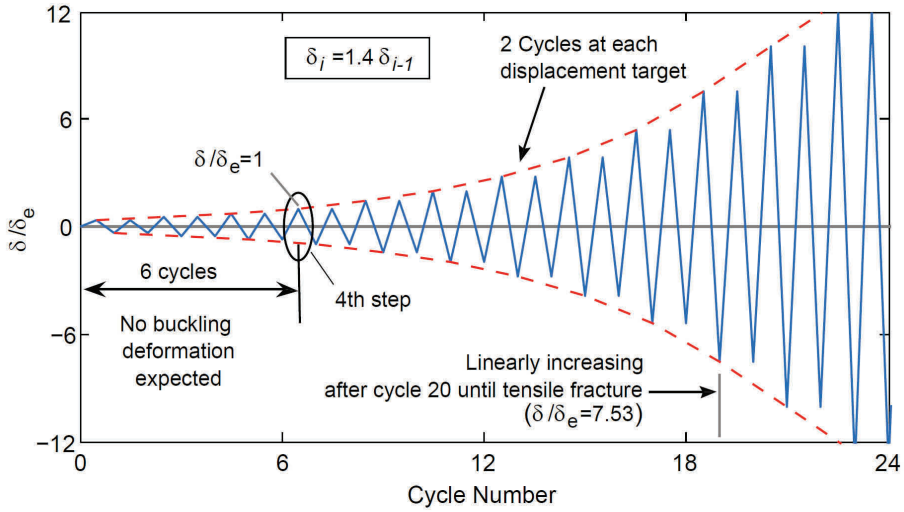

Figure 3: Cyclic loading protocol

5. Results

The cyclic hysteretic response for the 800S137-97 and 1200S162-97 are presented in Fig. 4, with the monotonic response overlaid to highlight trends in cyclic strength degradation. In Fig. 4, the experimental value of the rotation at the loading point is calculated as $\theta=\delta/a$, where δ is the average of the displacements measured at the loading points. This approximation is consistent with lumped-spring models for CFS flexural members, e.g. Ayhan et al. (2012). The elastic yielding rotation θ_y at the loading point corresponding to the yielding moment $M_y=SF_y$ is calculated as

$$\theta_y = \frac{M_y}{2EI}(L-2a) \tag{2}$$

For both cross-section types, the cyclic response starts with linear elastic deformation up to cycle 10, followed by out-of-plane lateral-torsional buckling deformation at cycle 15 which initiates local buckling of the compression flange, causing a rapid drop in capacity. The load deformation-response stabilizes at about $0.2M_y$ for both cross-section types, an interesting result important to seismic design. Even though the flanges have buckling and are not contributing to the flexural-torsional stiffness, the joist is still able to carry load for large deformations because the web and web-flange intersections experience compatibility-based membrane tension stiffening, see Fig. 5 and Virginia Tech's digital repository (VTechWorks 2013) for a video of the 800S137-97 cyclic test. Overall, the joist cyclic endurance is high, with no local fracture observed over 20 cycles.

Energy dissipation is observed to be similar for all specimens after peak load, i.e. for $\Sigma\theta/\theta_y > 10$, see Table 3. This trend was expected because the global slenderness of the 800S and 1200S specimens are similar, compare $M_{cre}=0.55M_y$ for the 800S specimens versus $M_{cre}=0.47M_y$ for the 1200S specimens. Similar member slenderness values (either global or cross-sectional) should produce similar magnitudes of energy dissipation based on recent observations by Padilla-Llano et. al. (2012). The total energy dissipated at the end of the tests however, differs for all specimens since the total number of cycles, therefore the cumulative deformation $\Sigma\theta/\theta_y$ (last column in Table 3), was different for each specimen. Pinching of the hysteretic response was less in the 1200S specimens than in the 800S specimens, a trend that occurs because there is more web material in the 1200S to provide torsional stiffness after the flanges have buckled.

Table 3: Hysteretic energy dissipated

Specimen	HE_{10} (kN-mm)	HE_{25} (kN-mm)	HE_{50} (kN-mm)	HE_{100} (kN-mm)	HE_T (kN-mm)	$max\ \Sigma\theta/\theta_y$
800S162-97-GFC-1	32	342	1056	2570	2818	107
800S162-97-GFC-2	61	304	1027	2573	3204	128
1200S162-97-GFC-1	29	379	1123	2486	4263	174
1200S162-97-GFC-2	24	370	977	2188	2500	114

$\max(\Sigma\theta/\theta_y)$ = cumulative deformation at the end of the test.

HE_{xx} = cumulative hysteretic energy dissipated up to $\Sigma\theta/\theta_y = xx$.

HE_T = cumulative hysteretic energy dissipated until failure.

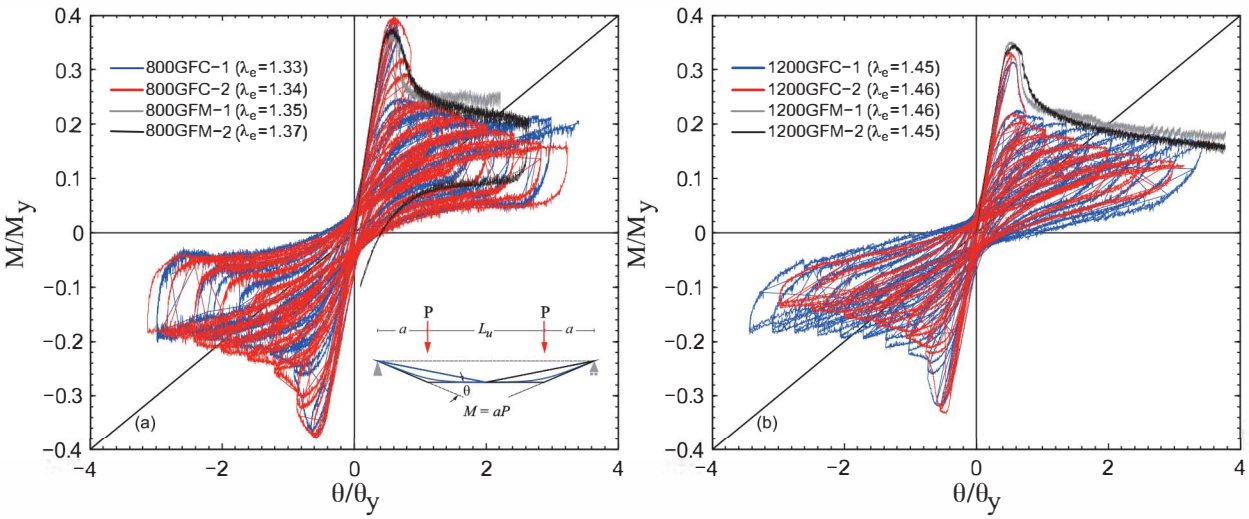

Figure 4: Monotonic and hysteretic cyclic response (a) 800S specimens, (b) 1200S specimens.

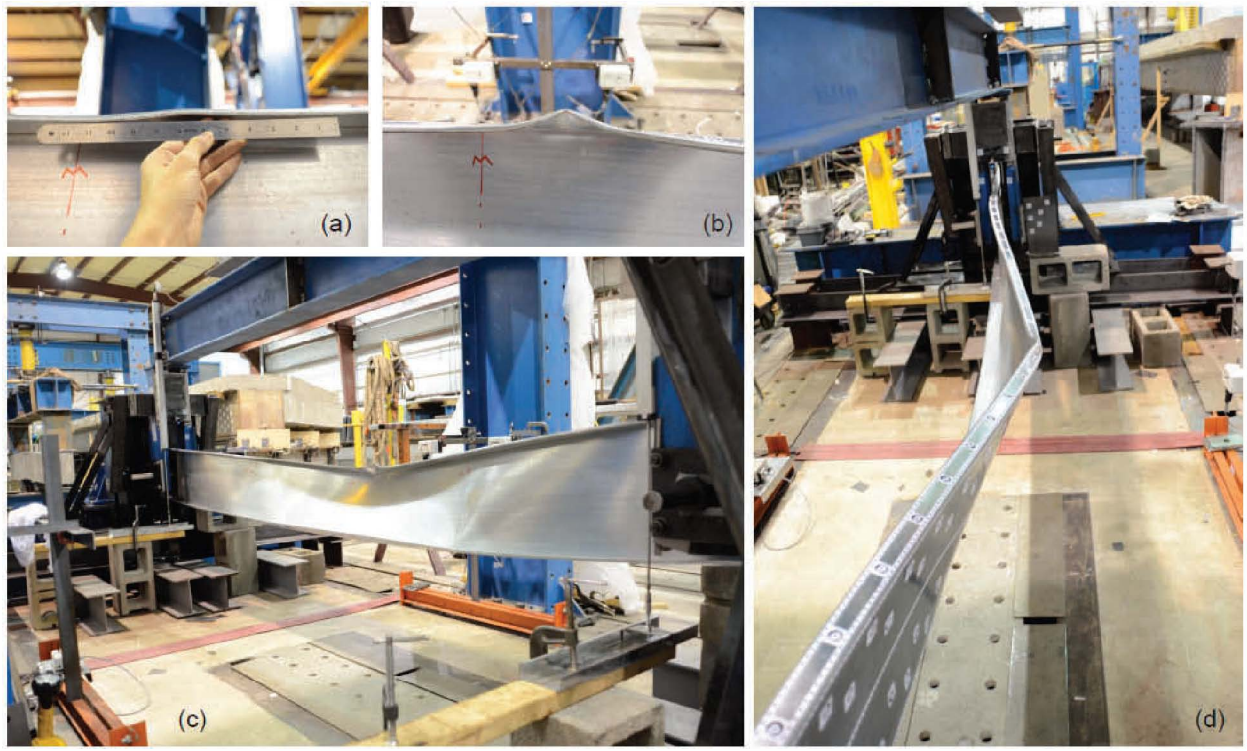

Figure 5: Specimen 1200S162-97-GFM-2, buckling of top flange (a); buckled top flange after peak moment (b); lateral torsional buckling (c, d)

The tested monotonic capacity provides insight into the accuracy of current code strength prediction assumptions (e.g., AISI-S100-07 Section C.3.1.2.1 or Appendix 1.2.2.1) and the validity of the warping fixed boundary condition assumption at the loading points. For the 800S specimens, the average M_{test}=6703kN-mm (M_{test}/M_n=0.69) for two specimens, while the average M_{test}=11405kN-mm (M_{test}/M_n=0.74) for the two 1200S joists. These results demonstrate that either the assumption that $M_{ne}=M_{cre}$ for $M_{cre}<0.56M_y$ is unconservative, or that the assumed boundary conditions (warping fixed, k=0.5) should be reconsidered. Sweep imperfections on the order of L/1495 were measured in all specimens and therefore it is expected that M_{test} should be

less than M_{cre}. Unconservative code-based predictions for cold-formed steel joists have been pointed out before (Put et al. 1999), adding supporting evidence that imperfections should be considered for beams in the elastic buckling range, in the same way that they are considered for columns (i.e., P_n=0.877P_{cre}). Finite element and analytical studies are underway to understand more about the boundary conditions and potentially refine the assumption of warping fixity. For example, if k=0.6 is assumed then M_{test}/M_n improves to 0.97 for the 800S specimen and 1.03 for the 1200S specimens.

6. Conclusions

Experiments were conducted to explore the cyclic performance and hysteretic response of unbraced cold-formed steel joists experiencing lateral-torsional buckling deformation. A drop in strength occurred when lateral movement of the compression flange resulted in top flange and lip buckling. However, even after the flanges buckled, in subsequent cycles the hysteretic loops remained consistent in size and shape, demonstrating that cold-formed steel joists can provide post-buckling stiffness and energy dissipation in a lateral-torsional buckling mode.

Acknowledgments

The authors are grateful to the American Iron and Steel Institute for supporting this project, and to Clark Dietrich Building Systems for the specimen donations.

References

Ayhan and Schafer (2012). "Characterization of moment-rotation response of cold-formed steel beams." *Proceedings of the Annual Stability Conference*, April 18-21, 2012, Grapevine, Texas.

Calderoni, B., De Martino, A., Formisano, A., Fiorino, L. (2009) "Cold Formed Steel Beams Under Monotonic and Cyclic Loading: Experimental Investigation." *Journal of Constructional Steel Research*, Vol. 65, pp. 219-227.

FEMA (2007). *Interim protocols for determining seismic performance characteristics of structural and nonstructural components through laboratory testing*, Published by the Federal Emergency Management Agency, Document No. FEMA 461.

Hsu, H.-L., Chi, P.-S. (2003). "Flexural Performance of Symmetrical Cold-Formed Thin-Walled Members Under Monotonic and Cyclic Loading." *Thin-Walled Structures*, Vol. 41, pp. 47-67.

Labview (2012). "Labview, Version 8". National Instruments, www.labview.com, Austin, TX.

Padilla-Llano D., Moen C. D., Eatherton M., McAnallen L., Bruce T. (2004). "Compression-Tension hysteretic response of cold-formed steel C-section framing members.", *Proceedings of the 21st International Specialty Conference on Cold-Formed Steel Structures*, October 24-25, 2012, St. Louis, Missouri.

Put, B., Pi, Y., and Trahair, N. (1999). "Lateral Buckling Tests on Cold-Formed Channel Beams." *J. Struct. Engineering.*, 125(5), 532–539.

R.L. Madsen, N. Nakata, B.W. Schafer (2011). *"CFS-NEES Building Structural Design Narrative"*, Research Report, RR01, access at www.ce.jhu.edu/cfsness, October 2011, revised RR01c May 2012.

VTechWorks (2013). <http://vtechworks.lib.vt.edu> (Feb, 2013)